nature nanotechnology

LETTERS

PUBLISHED ONLINE: 20 JUNE 2010 | DOI: 10.1038/NNANO.2010.132

Roll-to-roll production of 30-inch graphene films for transparent electrodes

Sukang Bae[1†], Hyeongkeun Kim[1,3†], Youngbin Lee[1], Xiangfan Xu[5], Jae-Sung Park[7], Yi Zheng[5], Jayakumar Balakrishnan[5], Tian Lei[1], Hye Ri Kim[2], Young Il Song[6], Young-Jin Kim[1,3], Kwang S. Kim[7], Barbaros Özyilmaz[5], Jong-Hyun Ahn[1,4]*, Byung Hee Hong[1,2]* and Sumio Iijima[1,8]

The outstanding electrical[1], mechanical[2,3] and chemical[4,5] properties of graphene make it attractive for applications in flexible electronics[6–8]. However, efforts to make transparent conducting films from graphene have been hampered by the lack of efficient methods for the synthesis, transfer and doping of graphene at the scale and quality required for applications. Here, we report the roll-to-roll production and wet-chemical doping of predominantly monolayer 30-inch graphene films grown by chemical vapour deposition onto flexible copper substrates. The films have sheet resistances as low as ~125 $\Omega\,\square^{-1}$ with 97.4% optical transmittance, and exhibit the half-integer quantum Hall effect, indicating their high quality. We further use layer-by-layer stacking to fabricate a doped four-layer film and measure its sheet resistance at values as low as ~30 $\Omega\,\square^{-1}$ at ~90% transparency, which is superior to commercial transparent electrodes such as indium tin oxides. Graphene electrodes were incorporated into a fully functional touch-screen panel device capable of withstanding high strain.

Conventional transparent electrodes make use of indium tin oxide (ITO) and are commonly used in solar cells, touch sensors and flat panel displays. It has a sheet resistance of less than 100 $\Omega\,\square^{-1}$, optical transparency of ~90%, and unlimited scalability. In contrast, the best reported sheet resistance of graphene grown on nickel substrates by chemical vapour deposition (CVD) is ~280 $\Omega\,\square^{-1}$ (refs 6,9,10), on the centimetre scale. Also, the CVD methods based on thermally deposited nickel thin films inevitably require a rigid substrate that can withstand temperatures close to ~1,000 °C and an etching process to remove the metal catalyst layers. These are therefore the main obstacles to the direct use of graphene on as-grown substrates[6,9,10]. Finding a way in which to transfer graphene films onto a foreign substrate is essential[11,12].

Recently, Li and colleagues discovered and demonstrated a CVD method that used centimetre-scale copper substrates[13], opening a new route to large-scale production of high-quality graphene films for practical applications. Graphene growth is therefore no longer limited to the use of rigid substrates; instead, large flexible copper foils may be used in the form of a roll-type substrate fitting inside a tubular furnace to maximize the scale and homogeneity of the produced graphene films. The flexibility of the graphene and copper foils further allows efficient etching and transfer processes that use a cost- and time-effective roll-to-roll production method. There are three essential steps in the roll-to-roll transfer[14–16] (Fig. 1a): (i) adhesion of polymer supports to the graphene on the copper foil; (ii) etching of the copper layers; and (iii) release of the graphene layers and transfer onto a target substrate. In the adhesion step, the graphene film, grown on a copper foil, is attached to a thin polymer film coated with an adhesive layer by passing between two rollers. In the subsequent step, the copper layers are removed by electrochemical reaction with aqueous 0.1 M ammonium persulphate solution $(NH_4)_2S_2O_8$ (ref. 17). Finally, the graphene films are transferred from the polymer support onto a target substrate by removing the adhesive force holding the graphene films. When using thermal release tapes[11,12], the graphene films are detached from the tapes and released to counter-substrates by thermal treatment (Fig. 1). The third step is not necessary when the target substrate is directly attached to the copper foil in the first step by permanent adhesion.

Figure 2a–c presents photographs of the roll-based synthesis and transfer process. An 8-inch-wide tubular quartz reactor (Fig. 2a) is used in the CVD system, allowing a monolayer graphene film to be synthesized on a roll of copper foil with dimensions as large as 30 inches in the diagonal direction (Fig. 2c). A temperature gradient usually exists that depends on the radial position inside the tubular reactor. In our preliminary work, this sometimes resulted in inhomogeneous growth of the graphene on the copper foils. To solve this problem, a ~7.5-inch quartz tube wrapped with a copper foil was inserted and suspended inside the 8-inch quartz tube. In this way, the radial inhomogeneity in the reaction temperature could be minimized (Supplementary Fig. S1). In the first step of synthesis, the roll of copper foil is inserted into a tubular quartz tube and then heated to 1,000 °C with flowing 8 s.c.c.m. H_2 at 90 mtorr. After reaching 1,000 °C, the sample is annealed for 30 min without changing the flow rate or pressure. The copper foils are heat-treated to increase the grain size from a few micrometres to ~100 μm, as we have found that the copper foils with larger grain size yield higher-quality graphene films, as suggested by Li and colleagues[13] (Supplementary Fig. S3). The gas mixture of CH_4 and H_2 is then flowed at 460 mtorr with rates of 24 and 8 s.c.c.m. for 30 min, respectively. Finally, the sample is rapidly cooled to room temperature (~10 °C s^{-1}) with flowing H_2 under a pressure of 90 mtorr.

After growth, the graphene film grown on copper foil is attached to a thermal release tape (Jinsung Chemical Co. and Nitto Denko

[1]SKKU Advanced Institute of Nanotechnology (SAINT) and Center for Human Interface Nano Technology (HINT), Sungkyunkwan University, Suwon 440-746, Korea, [2]Department of Chemistry, Sungkyunkwan University, Suwon 440-746, Korea, [3]School of Mechanical Engineering, Sungkyunkwan University, Suwon 440-746, Korea, [4]School of Advanced Materials Science and Engineering, Sungkyunkwan University, Suwon 440-746, Korea, [5]NanoCore & Department of Physics, National University of Singapore, Singapore 117576 & 117542, [6]Digital & IT Solution Division, Samsung Techwin, Seongnam 462-807, Korea, [7]Center for Superfunctional Materials, Department of Chemistry, Pohang University of Science and Technology, Hyojadong, Namgu, Pohang 790-784, Korea, [8]Nanotube Research Center, National Institute of Advanced Industrial Science and Technology (AIST), Tsukuba 305-8565 & Faculty of Science and Engineering, Meijo University, Nagoya 468-8502, Japan; †These authors contributed equally to this work.
*e-mail: byunghee@skku.edu; ahnj@skku.edu

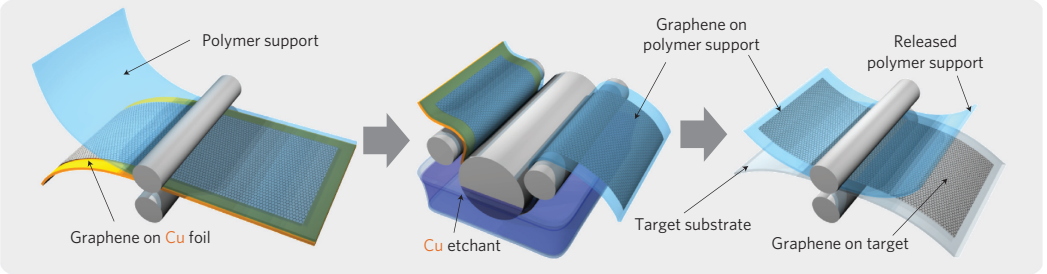

Figure 1 | Schematic of the roll-based production of graphene films grown on a copper foil. The process includes adhesion of polymer supports, copper etching (rinsing) and dry transfer-printing on a target substrate. A wet-chemical doping can be carried out using a set-up similar to that used for etching.

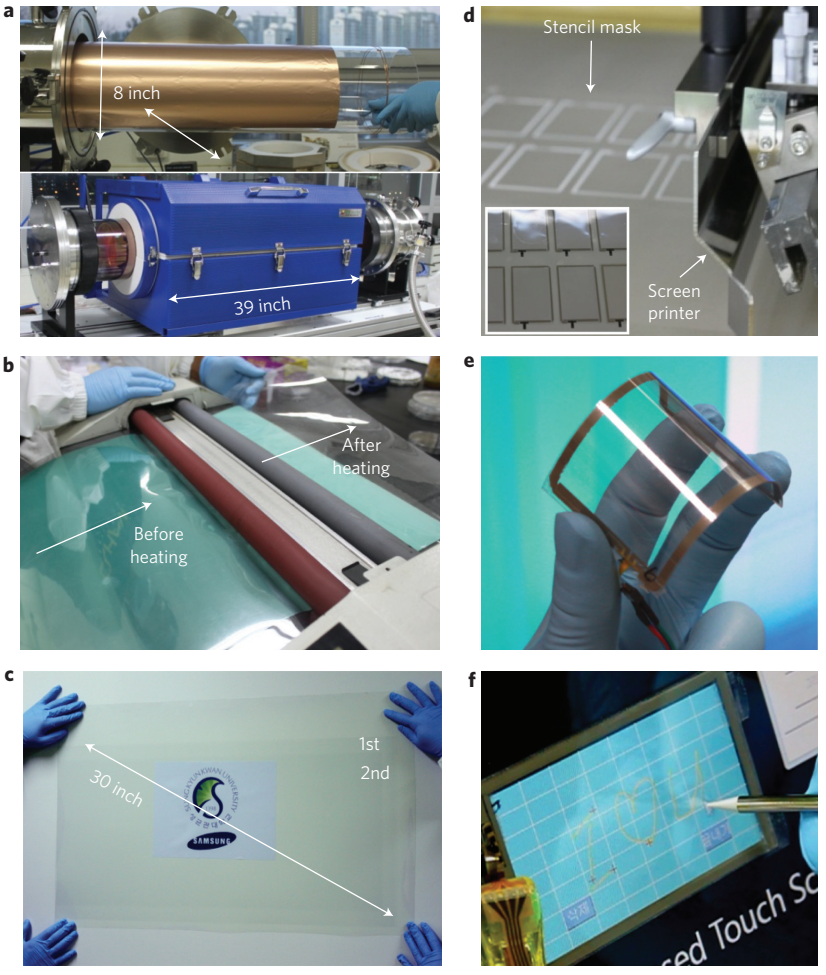

Figure 2 | Photographs of the roll-based production of graphene films. a, Copper foil wrapping around a 7.5-inch quartz tube to be inserted into an 8-inch quartz reactor. The lower image shows the stage in which the copper foil reacts with CH_4 and H_2 gases at high temperatures. **b**, Roll-to-roll transfer of graphene films from a thermal release tape to a PET film at 120 °C. **c**, A transparent ultralarge-area graphene film transferred on a 35-inch PET sheet. **d**, Screen printing process of silver paste electrodes on graphene/PET film. The inset shows 3.1-inch graphene/PET panels patterned with silver electrodes before assembly. **e**, An assembled graphene/PET touch panel showing outstanding flexibility. **f**, A graphene-based touch-screen panel connected to a computer with control software. For a movie of its operation see Supplementary Information.

Co.) by applying soft pressure (~0.2 MPa) between two rollers. After etching the copper foil in a plastic bath filled with copper etchant, the transferred graphene film on the tape is rinsed with deionized water to remove residual etchant, and is then ready to be transferred to any kind of flat or curved surface on demand. The graphene film on the thermal release tape is inserted between the rollers together with a target substrate and exposed to mild heat (~90–120 °C), achieving a transfer rate of ~150–200 mm min^{-1} and resulting in the transfer of the graphene films from the tape to the target substrate (Fig. 2b). By repeating these steps on the same substrate, multilayered graphene films can be prepared that exhibit enhanced electrical and optical properties, as demonstrated by Li and colleagues using wet-transfer methods at the centimetre scale[19]. Figure 2c shows the 30-inch multilayer graphene film transferred to a roll of 188-μm-thick polyethylene terephthalate (PET) substrate. Figure 2d shows a screen-printing process used to fabricate four-wire touch-screen panels[18] based on graphene/PET transparent conducting films

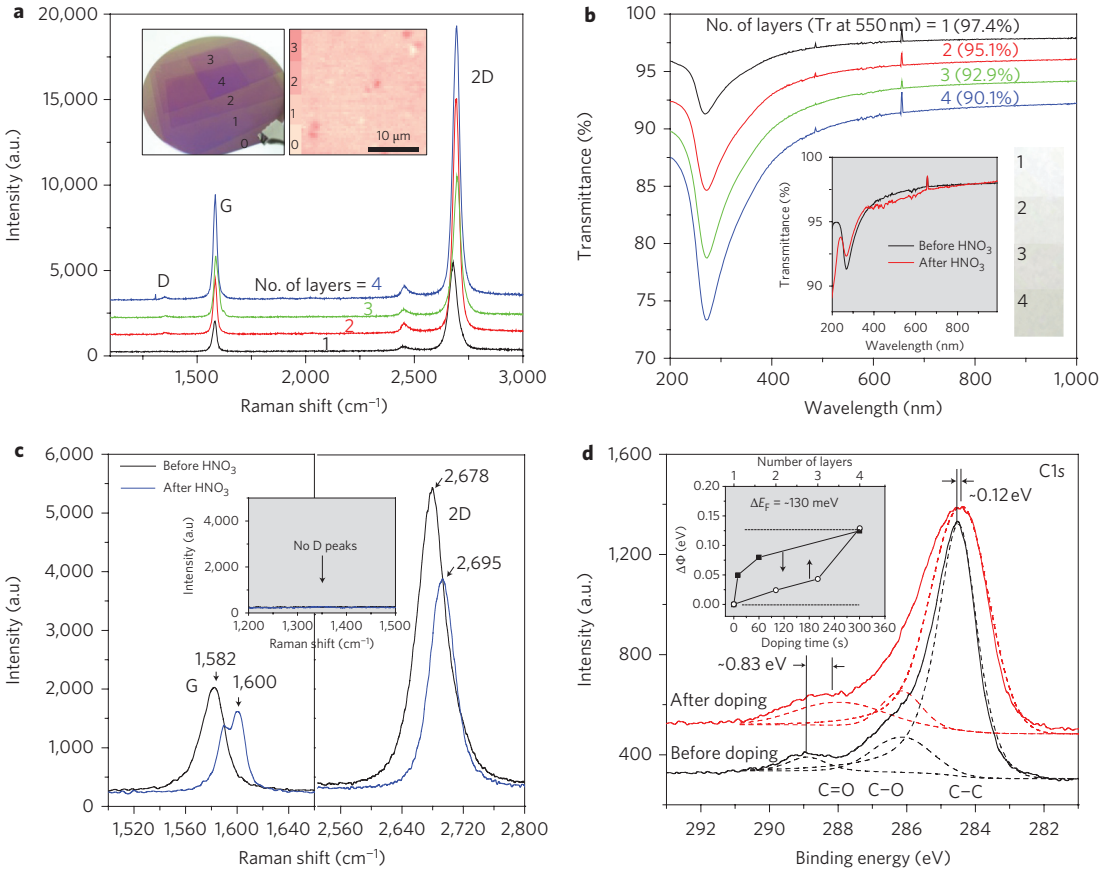

Figure 3 | Optical characterizations of the graphene films prepared using layer-by-layer transfer on SiO_2/silicon and PET substrates. a, Raman spectra of graphene films with different numbers of stacked layers. The left inset shows a photograph of transferred graphene layers on a 4-inch SiO_2(300 nm)/silicon wafer. The right inset is a typical optical microscope image of the monolayer graphene, showing >95% monolayer coverage. A PMMA-assisted transfer method is used for this sample. **b**, UV–vis spectra of roll-to-roll layer-by-layer transferred graphene films on quartz substrates. The inset shows the UV spectra of graphene films with and without HNO_3 doping. The right inset shows optical images for the corresponding number of transferred layers (1×1 cm^2). The contrast is enhanced for clarity. **c**, Raman spectra of HNO_3-doped graphene films, showing ~18 cm^{-1} blueshift both for G and 2D peaks. D-band peaks are not observed before or after doping, indicating that HNO_3 treatment is not destructive to the chemical bonds of graphene. **d**, XPS peaks of monolayer graphene films transferred on SiO_2/Si substrates, showing typical redshift and broadening of carbon 1*s* peaks (C1*s*) caused by p-doping. The inset shows work-function changes ($\Delta\Phi$) with respect to doping time (lower *x*-axis) and number of stacked layers (upper *x*-axis), measure by UPS.

(Supplementary Fig. S12). After printing electrodes and dot spacers, the upper and lower panels are carefully assembled and connected to a controller installed in a laptop computer (Fig. 2e–f), which shows extraordinary flexibility as we will discuss later (Fig. 4d). The scalability and processability of CVD graphene and the roll-to-roll methods presented here are expected to enable the continuous production of graphene-based electronic devices at large scales.

The graphene films seem to be predominantly composed of monolayers when analysed using Raman spectra (Fig. 3a). However, atomic force microscope (AFM) and transmission electron microscope (TEM) images often show bilayer and multilayer islands (Supplementary Figs S5,S6). As the graphene layers are transferred one after another[19], the intensities of the G- and 2D-band peaks increase together, but their ratios do not change significantly. This is because the hexagonal lattices of the upper and lower layers are randomly oriented, unlike in graphite, so the original properties of each monolayer remain unchanged, even after stacking into multilayers[20,21]; this is clearly different from the case of multilayer graphene exfoliated from graphite crystals[22]. The randomly stacked layers behave independently without significant change in the electronic band structures, and the overall conductivity of the graphene films appears to be proportional to the number of stacked layers[19]. The optical transmittance is usually reduced by ~2.2–2.3% for an additional transfer, implying that the average thickness is approximately a monolayer (Fig. 3b)[23].

The unique electronic band structure of graphene allows modulation of the charge carrier concentrations in dependence on an electric field induced by gate bias[24] or chemical doping[25], resulting in enhancement of sheet resistance. We tried various types of chemical doping methods, and found that nitric acid (HNO_3) is very effective for p-doping of graphene films (Supplementary Fig. S10). Figure 3c shows Raman spectra of the graphene films before and after doping with 63 wt% HNO_3 for 5 min. The large peak shift ($\Delta\nu = 18$ cm^{-1}) indicates that the graphene film is strongly p-doped. The shifted G peak is often split near the randomly stacked bilayer islands, as shown in Fig. 3c. We hypothesize that the lower graphene layer, which is screened by top layers, experiences a reduced doping effect, leading to G-band splitting. In X-ray photoelectron spectra (XPS), the C1*s* peaks corresponding to sp^2 and sp^3 hybridized states are shifted to lower energy, similar to the case for p-doped carbon nanotubes[25]. However, multilayer stacking results in blueshifted C1*s* peaks. We suppose that weak chemical bonding such as the π–π stacking interaction causes descreening of nucleus charges, leading to an overall increase in core electron binding energies. We also find that the work functions of graphene films as estimated by UV photoelectron spectroscopy (UPS) are blueshifted by ~130 meV with increasing doping time

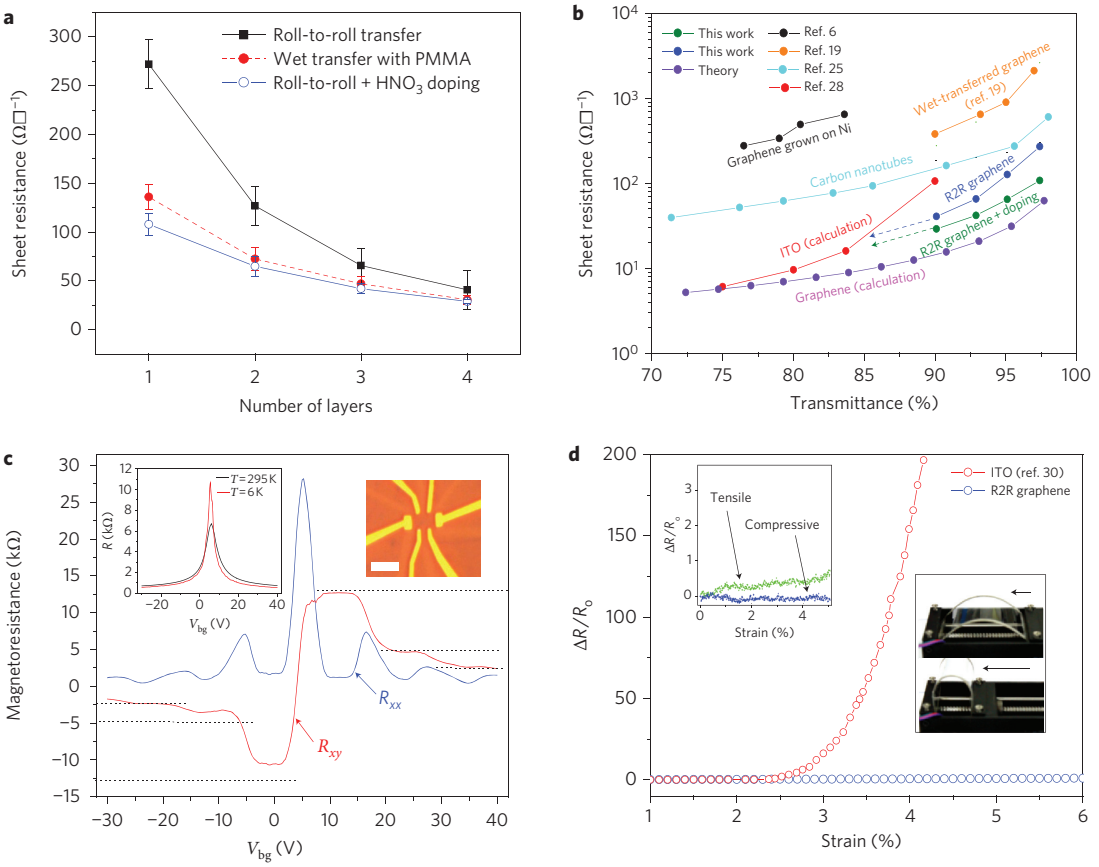

Figure 4 | Electrical characterizations of layer-by-layer transferred and HNO_3-doped graphene films. a, Sheet resistances of transferred graphene films using a roll-to-roll (R2R) dry-transfer method combined with thermal release tapes and a PMMA-assisted wet-transfer method. **b**, Comparison of sheet resistance from this research and transmittance plots taken from other references. The dashed arrows indicate the expected sheet resistances at lower transmittance. The scheme is borrowed from ref. 19. **c**, Electrical properties of a monolayer graphene Hall bar device in vacuum. Four-probe resistivity (left bottom inset) is measured as a function of gate voltage in the monolayer graphene Hall bar shown in the right inset at room temperature (black curve) and $T = 6$ K (red curve). The QHE effect at $T = 6$ K and $B = 9$ T is measured in the same device. The longitudinal resistivity ρ_{xx} and Hall conductivity σ_{xy} are plotted as a function of gate voltage. The sequence of the first three half-integer plateaus corresponding to $\nu = 2$, 6 and 10, typical for single-layer graphene, are clearly seen. The Hall effect mobility of this device is $\mu_{Hall} = 7{,}350\ cm^{-2}\ V^{-1}\ s^{-1}$ at 6 K (~5,100 $cm^{-2}\ V^{-1}s^{-1}$ at 295 K). Scale bar (inset), 3 μm. **d**, Electromechanical properties of graphene-based touch-screen devices compared with ITO/PET electrodes under tensile strain. The inset shows the resistance change with compressive and tensile strain applied to the upper and lower graphene/PET panels, respectively.

(Fig. 3d, inset). The multiple stacking also changes the work functions (Fig. 3d, inset; see also Supplementary Fig. S7 and Table S1), which could be very important in controlling the efficiency of photovoltaic[26] or light-emitting devices based on graphene transparent electrodes[27].

The electrical properties of graphene films formed using layer-by-layer stacking methods were also investigated. Usually, the sheet resistance of graphene film with 97.4% transmittance is as low as ~125 $\Omega\square^{-1}$ (Fig. 4a) when it is transferred by a soluble polymer support such as polymethyl methacrylate (PMMA)[9,10,19]. The transferrable size achievable using wet-transfer methods is limited to less than a few inches of wafer because of the weak mechanical strength of spin-coated PMMA layers. However, the scale of roll-to-roll dry transfer assisted by a thermal release tape is in principle unlimited. In the process of roll-to-roll dry transfer, the first layer sometimes shows approximately two to three times larger sheet resistance than that of the PMMA-assisted wet-transfer method. As the number of layers increases, the resistance drops faster compared to the wet-transfer method (Fig. 4a). We postulate that the adhesion of the first layer with the substrate is not strong enough for complete separation of the graphene films from the thermal release tapes (Supplementary Fig. S4). As a result, there can be mechanical damage on the graphene films, leading to an increase in the overall sheet resistance. Because additional layers are not directly affected by the adhesion with the substrate surface, the sheet resistance of multilayers prepared by the roll-to-roll method does not differ much from that for the wet-transfer case. The p-doping with HNO_3 clearly enhances the electrical properties of graphene films, and is more effective in roll-to-roll processes. The sheet resistance of the p-doped four-layer graphene film with ~90% optical transmittance is as low as ~30 $\Omega\square^{-1}$, which is superior to common transparent electrodes such as ITO and carbon-nanotube films (Fig. 4b)[28].

Standard electron-beam lithography has been used to fabricate graphene Hall bars on conventional 300-nm SiO_2/Si substrates (Fig. 4c). The left inset of Fig. 4c shows the four-terminal resistance of such samples as a function of backgate voltage (V_{bg}) at both room temperature (in black) and at a low temperature ($T = 6$ K) and zero magnetic field. We observe the graphene specific gate bias dependence of the resistance with a sharp Dirac peak and an effective Hall mobility of 7,350 $cm^2\ V^{-1}\ s^{-1}$ at low temperatures. This allows the observation of the quantum Hall effect (QHE)[29] at 6 K and a magnetic field of $B = 9$ T (Fig. 4c, right). The fingerprint of single-layer graphene, the half-integer quantum Hall effect, is observed with plateaus at filling factors of $\nu = 2$, 6 and 10 at $R_{xy} = \frac{1}{2}, \frac{1}{6}$ and $\frac{1}{10}(h/e^2)$, respectively. Although the sequence of

the plateaus remains for both the electron side and the hole side, there is a slight deviation from the fully quantized values on the hole side.

Finally, the electromechanical properties of graphene/PET touch-screen panels were tested (Fig. 4d; Supplementary Fig. S2). Unlike an ITO-based touch panel, which easily breaks under ~2–3% strain, the graphene-based panel resists up to 6% strain; this is limited not by the graphene itself, but by the printed silver electrodes (Fig. 4d)[30].

In summary, we have developed and demonstrated the roll-to-roll production of graphene on ultralarge copper substrates. The multiple transfer and simple chemical doping of graphene films considerably enhances its electrical and optical properties. Given the scalability and processability of roll-to-roll and CVD methods and the flexibility and conductivity of graphene films, we anticipate that the commercial production of large-scale transparent electrodes, replacing ITO, will be realized in the near future.

Received 11 March 2010; accepted 28 May 2010;
published online 20 June 2010; corrected online 25 June 2010

References

1. Geim, A. K. & Novoselov, K. S. The rise of graphene. *Nature Mater.* **6,** 183–191 (2007).
2. Lee, C., Wei, X., Kysar, J. W. & Hone, J. Measurement of the elastic properties and intrinsic strength of monolayer graphene. *Science* **321,** 385–388 (2008).
3. Bunch, J. S. *et al.* Impermeable atomic membranes from graphene sheets. *Nano Lett.* **8,** 2458–2462 (2008).
4. Elias, D. C. *et al.* Control of graphene's properties by reversible hydrogenation: evidence for graphene. *Science* **323,** 610–613 (2009).
5. Wang, X. *et al.* N-doping of graphene through electrothermal reactions with ammonia. *Science* **324,** 768–771 (2009).
6. Kim, K. S. *et al.* Large-scale pattern growth of graphene films for stretchable transparent electrodes. *Nature* **457,** 706–710 (2009).
7. Kim, D.-H. *et al.* Stretchable and foldable silicon integrated circuits. *Science* **320,** 507–511 (2008).
8. Sekitani, T. *et al.* A rubberlike stretchable active matrix using elastic conductors. *Science* **321,** 1468–1472 (2008).
9. Reina, A. *et al.* Large area, few-layer graphene films on arbitrary substrates by chemical vapor deposition. *Nano Lett.* **9,** 30–35 (2009).
10. Cai, W. W. *et al.* Large area few-layer graphene/graphite films as transparent thin conducting electrodes. *Appl. Phys. Lett.* **95,** 123115 (2009).
11. Lee, Y. *et al.* Wafer-scale synthesis and transfer of graphene films. *Nano Lett.* **10,** 490–493 (2010).
12. Caldwell, J. D. *et al.* Technique for the dry transfer of epitaxial graphene onto arbitrary substrates. *ACS Nano* **4,** 1108–1114 (2010).
13. Li, X. *et al.* Large-area synthesis of high-quality and uniform graphene films on copper foils. *Science* **324,** 1312–1314 (2009).
14. Ahn, S. H. & Guo, L. J. High-speed roll-to-roll nanoimprint lithography on flexible plastic substrates. *Adv. Mater.* **20,** 2044–2049 (2008).
15. Yerushalmi, R., Jacobson, Z. A., Ho, J. C., Fan, Z. & Javey, A. Large scale, highly ordered assembly of nanowire parallel arrays by differential roll printing. *Appl. Phys. Lett.* **91,** 203104 (2007).
16. Chang, Y. K. & Hong, F. C. The fabrication of ZnO nanowire field-effect transistors by roll-transfer printing. *Nanotechnology* **20,** 195302 (2009).
17. Jo, G. *et al.* Etching solution for etching Cu and Cu/Ti metal layer of liquid crystal display device and method of fabricating the same. US patent, 6,881,679 (2005).
18. Hecht, D. S. *et al.* Carbon nanotube film on plastic as transparent electrode for resistive touch screens. *J. Soc. Inf. Display* **17,** 941–946 (2009).
19. Li, X. *et al.* Transfer of large-area graphene films for high-performance transparent conductive electrodes. *Nano Lett.* **9,** 4359–4363 (2009).
20. Hass, J. *et al.* Why multilayer graphene on 4H-SiC(000–1) behaves like a single sheet of graphene. *Phys. Rev. Lett.* **100,** 125504 (2008).
21. Sprinkle, M. *et al.* First direct observation of a nearly ideal graphene band structure. *Phys. Rev. Lett.* **103,** 226803 (2009).
22. Ferrari, A. C. *et al.* Raman spectrum of graphene and graphene layers. *Phys. Rev. Lett.* **97,** 187401 (2006).
23. Nair, R. R. *et al.* Fine structure constant defines visual transparency of graphene. *Science* **320,** 1308 (2008).
24. Das, A. *et al.* Monitoring dopants by Raman scattering in an electrochemically top-gated graphene transistor. *Nature Nanotech.* **3,** 210–215 (2008).
25. Geng, H.-Z. *et al.* Effect of acid treatment on carbon nanotube-based flexible transparent conducting films. *J. Am. Chem. Soc.* **129,** 7758–7759 (2007).
26. Schrivera, M., Reganb, W., Losterb, M. & Zettl, A. Carbon nanostructure–aSi:H photovoltaic cells with high open-circuit voltage fabricated without dopants. *Solid State Commun.* **150,** 561–563 (2010).
27. Wu, J. *et al.* Organic light-emitting diodes on solution-processed graphene transparent electrodes. *ACS Nano* **4,** 43–48 (2010).
28. Lee, J.-Y., Connor, S. T., Cui, Y. & Peumans, P. Solution-processed metal nanowire mesh transparent electrodes. *Nano Lett.* **8,** 689–692 (2008).
29. Cao, H. L. *et al.* Electronic transport in chemical vapor deposited graphene synthesized on Cu: Quantum Hall effect and weak localization. *Appl. Phys. Lett.* **96,** 122106 (2010).
30. Cairns, D. R. *et al.* Strain-dependent electrical resistance of tin-doped indium oxide on polymer substrates. *Appl. Phys. Lett.* **76,** 1425–1427 (2000).

Acknowledgements

This work was supported by the National Research Foundation of Korea (NRF), funded by the Ministry of Education, Science and Technology (2009-0081966, 2009-0082608, 2009-0083540, 2009-0090017, World Class University R33-2008-000-10138-0, National Honor Scientist Program), the Research Centre of Breakthrough Technology Program through the Korea Institute of Energy Technology Evaluation and Planning (KETEP), funded by the Ministry of Knowledge Economy (2009-3021010030-11-1), Singapore National Research Foundation (NRF-RF2008-07) & NUS NanoCore, and T.J. Park Junior Faculty Fellowship. The authors thank R. Ruoff (University of Texas at Austin) and P. Kim (Columbia University) for helpful comments, W.S. Lim, K.D. Kim and Y.D. Kim (SKKU) for assistance in XPS analysis, and Samkwang Well Tech Co. for assistance with the touch-panel fabrication.

Author contributions

B.H.H. planned and supervised the project, with assistance in supervision from J.H.A. Y.-J.K., B.O., K.S.K. and S.I. provided advice for the project. B.H.H., S.B. and H.K. conceived and carried out the experiment. B.H.H., J.H.A. and B.O. analysed the data and wrote the manuscript. X.X., J.B., Y.Z. and B.O. fabricated the QHE devices, and carried out the measurements. Y.L. and Y.I.S. helped with the fabrication of touch-screen panels and electromechanical analysis. J.S.P., H.R.K. and T.L. helped with the doping experiment.

Additional information

The authors declare no competing financial interests. Supplementary information accompanies this paper at www.nature.com/naturenanotechnology. Reprints and permission information is available online at http://npg.nature.com/reprintsandpermissions/. Correspondence and requests for materials should be addressed to B.H.H. and J.H.A.

ERRATUM

Roll-to-roll production of 30-inch graphene films for transparent electrodes

Sukang Bae, Hyeongkeun Kim, Youngbin Lee, Xiangfan Xu, Jae-Sung Park, Yi Zheng, Jayakumar Balakrishnan, Tian Lei, Hye Ri Kim, Young Il Song, Young-Jin Kim, Kwang S. Kim, Barbaros Özyilmaz, Jong-Hyun Ahn, Byung Hee Hong and Sumio Iijima

Nature Nanotechnology doi:10.1038/nnano.2010.132 (2010); published online: 20 June 2010; corrected after print: 25 June 2010.

In the PDF version of this Letter originally published online, the authors were listed incorrectly. This error has now been corrected.

nature nanotechnology

SUPPLEMENTARY INFORMATION

DOI: 10.1038/NNANO.2010.132

Roll-to-roll production of 30-inch graphene films for transparent electrodes

Sukang Bae, Hyeongkeun Kim, Youngbin Lee, Xianfang Xu, Jae-Sung Park, Yi Zheng, Jayakumar Balakrishnan, Tian Lei, Hye Ri Kim, Young Il Song, Young-Jin Kim, Kwang S. Kim, Barbaros Özyilmaz, Jong-Hyun Ahn, Byung Hee Hong & Sumio Iijima

DOI: 10.1038/NNANO.2010.132

A. Homogeneity analysis of a large-scale graphene film

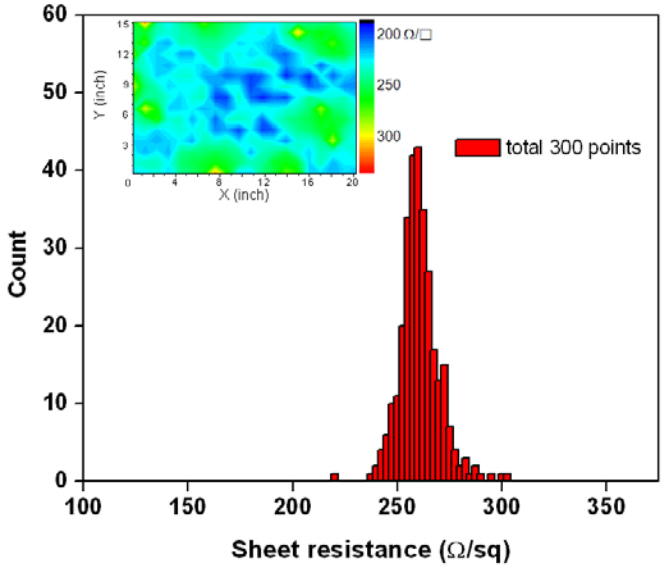

Fig. S1. Distribution of sheet resistances tested on the 300 pieces of 1x1 inch^2 monolayer graphene/PET films. The inset shows the corresponding spatial distribution on a 20x15 inch^2 graphene/PET film.

B. Strain analysis of graphene electrodes

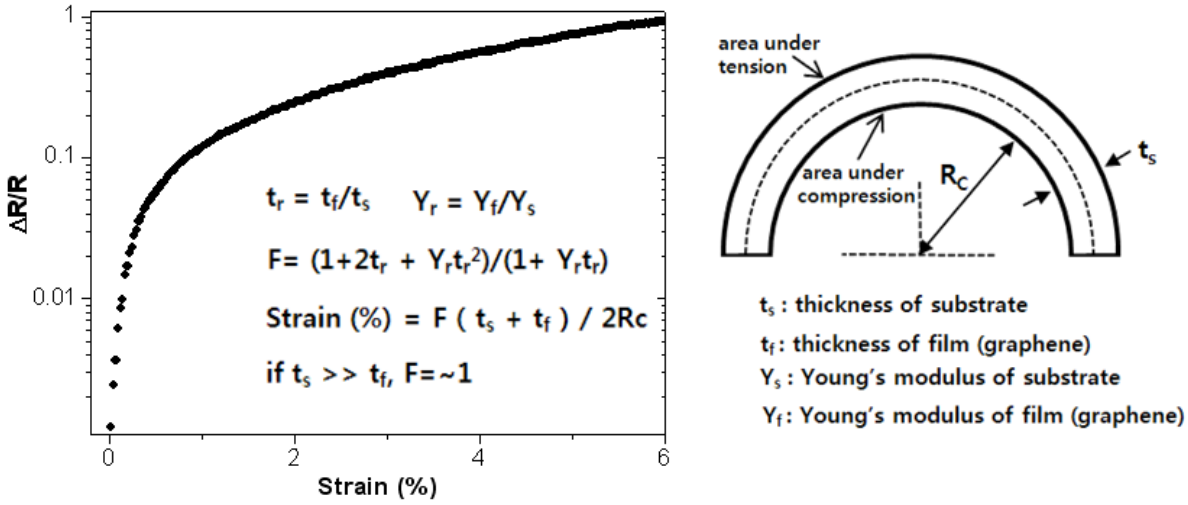

Fig S2. Log-scaled *ΔR/R vs. strain* plot for a graphene electrode used in touch screen panel devices. The parameters and equations from *Ref. S1* are used to calculate the strain. Note that we can simply use F = ~1 in the case of ultrathin film on a thick substrate.

S1) Z. Suo, E. Y. Ma, H. Gleskova, S. Wagner. Mechanics of rollable and foldable film-on-foil electronics. *Appl. Phys. Lett*. **74**, 1177 (1999).

C. Enlarged grain sizes of Cu foil after annealing/growth

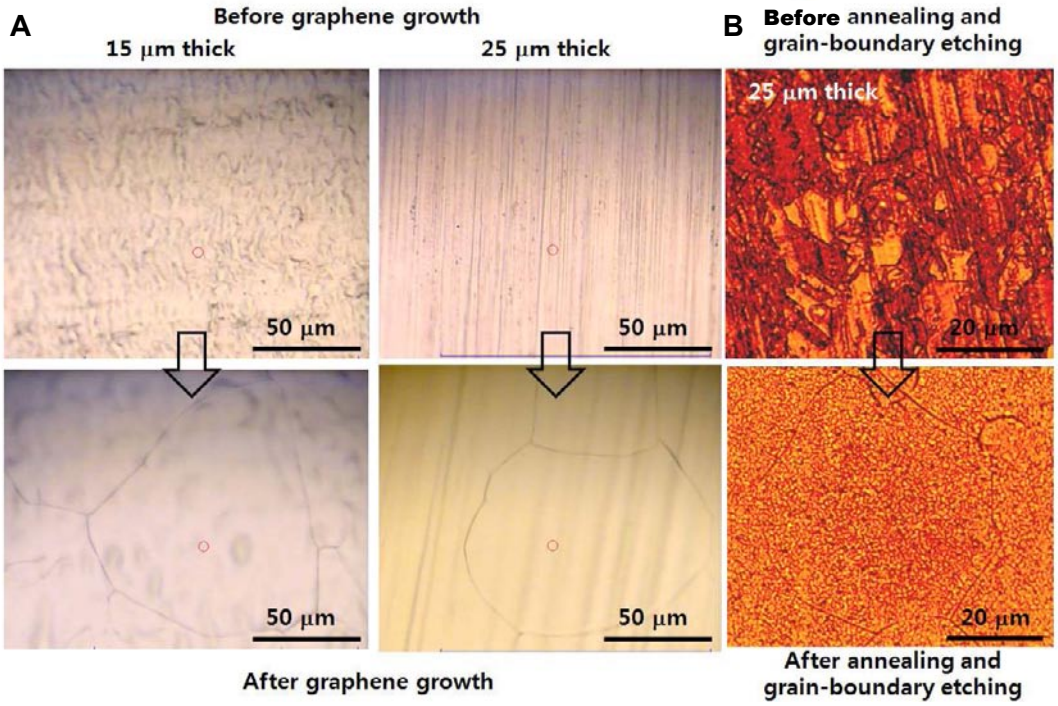

Fig. S3. Grain size analyses of Cu foils before and after annealing/growth. (**A**) Optical microscope images of Cu foils before and after graphene growth at 1,000°C. The cracks on foils usually formed at grain boundaries. (**B**) Optical images of polished Cu foils before and after annealing at 1,000°C, followed by brief acid treatment. The grain boundaries are etched faster than single crystalline surfaces, resulting in the formation line patterns on the polished Cu surface.

D. SEM images of transferred graphene films

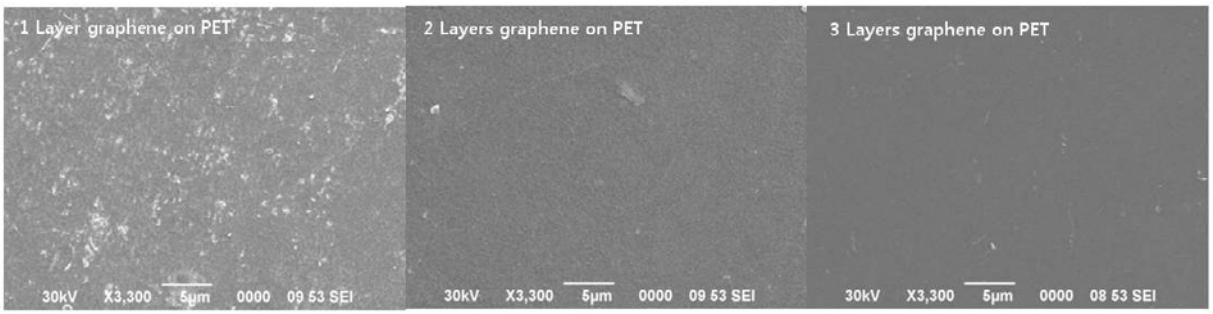

Fig. S4. SEM images of 1~3-layer graphene films transferred on a PET by a roll-to-roll method. The first transferred graphene layer shows adhesive residues, while the additional transfers look very clean. We supposed that the adhesion force between graphene and PET competes with the force between graphene and thermal release tapes, leaving some adhesive residues and defects. In the case of the second/third transfer, the adhesive forces of thermal release tapes look much smaller than graphene-graphene adhesion, and therefore, almost complete transfer can be made for additional transfers.

DOI: 10.1038/NNANO.2010.132

E. AFM analysis of graphene films

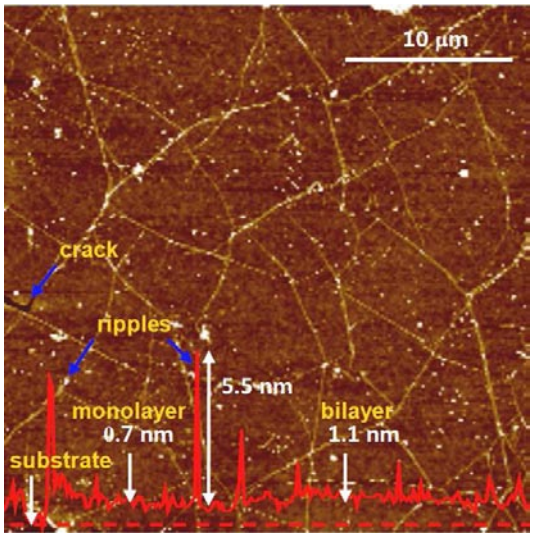

Fig. S5. A contact-mode AFM image of the graphene film transferred on a PET film. A few nm high ripples are usually formed due to the different thermal expansion of Cu and graphene, and the cracks are formed during transfer process. The height profile (red solid line) measured along the dashed red line indicates the thicknesses of mono- and bi-layers approximately.

F. TEM images of as-grown graphene films

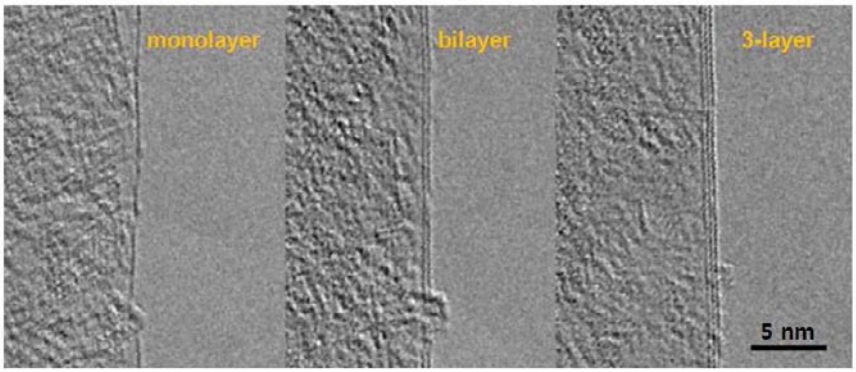

Fig. S6. High-resolution TEM images showing the folded edges of as-grown graphene films with different number of layers.

G. Ultraviolet photoelectron spectroscopy (UPS) analysis of graphene films

Table S1. Work functions (*eV*) of multiple transferred graphene films measured by UPS.

No. transfer	1	2	3	4
before HNO_3 doping	*4.272	4.296	4.315	4.401
after HNO_3 doping	4.414	4.462	4.476	4.489

*The work functions of single-layer and bilayer graphene measured by scanning Kelvin probe microscopy (SKPM) are 4.57 eV and 4.69 eV respectively (*Ref.* Y. Yu *et al. Nano Lett*. **9**, 3430 (2009)).

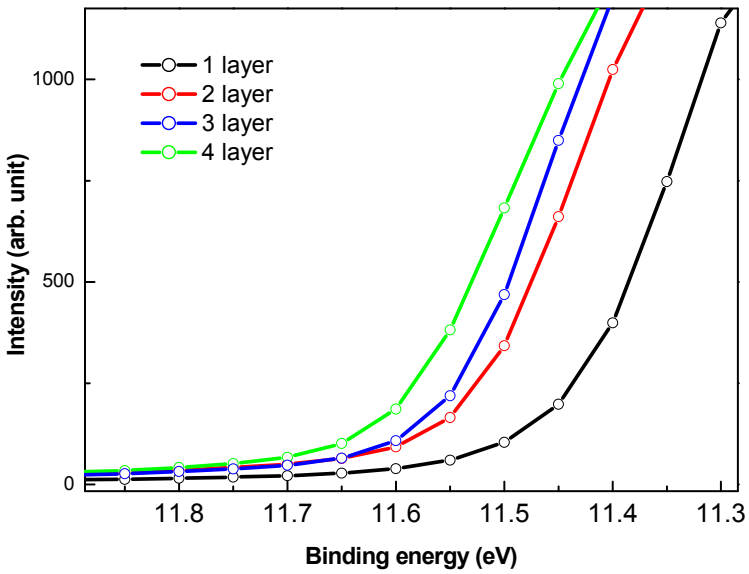

Fig. S7. UPS spectra of HNO_3-doped graphene films with different number of stacked layers. The binding energy increases with the number of stacked graphene layers.

H. XPS spectra of transferred 2-layer graphene films

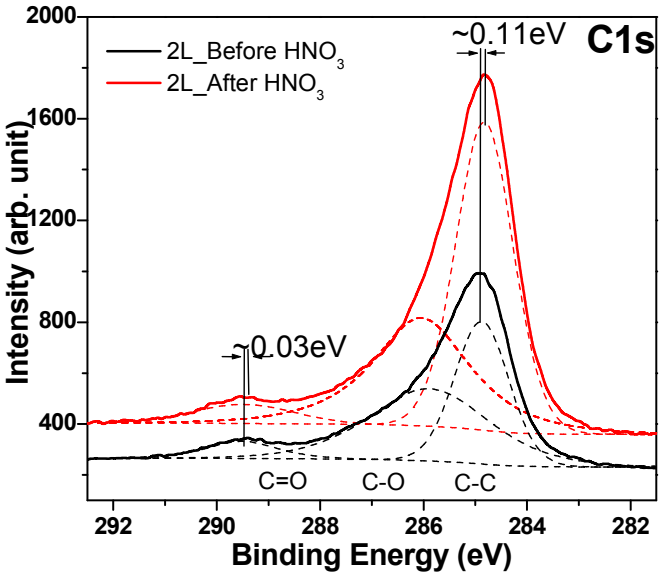

Fig S8. XPS spectra of 2-monolayer graphene films transferred on SiO_2 substrates. The black and red lines denote the XPS spectra before and after HNO_3 doping, respectively. The higher energy C1s peaks related to carbon-oxygen bonds are often observed in CVD-grown graphene samples, which is probably due to oxygen and amorphous carbon contamination inside the growth chamber.

DOI: 10.1038/NNANO.2010.132

I. Origin of low sheet resistance

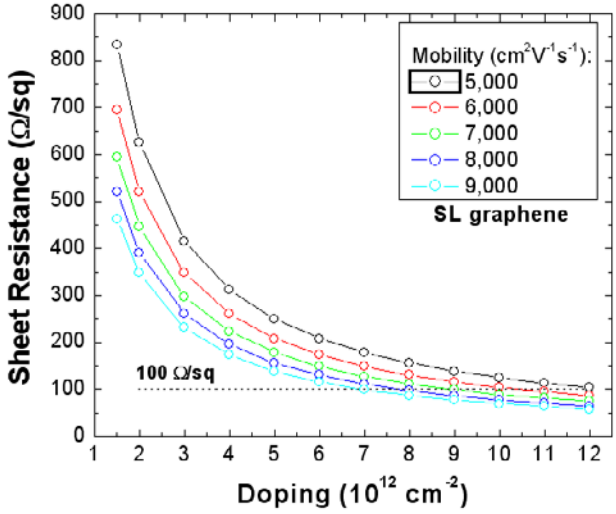

Fig S9. Sheet resistance vs. doping with different charge carrier mobility. The sheet resistance is calculated by $\rho = 1/\sigma = 1/ne\mu$. During the etching process, the graphene can be *p*-doped by etchants such as ammonium persulfate or iron chloride. These etchants are usually strong oxidizing agents. Therefore, the electrons can be withdrawn from graphene during the redox process, which is supposed to be the reason for the low sheet resistance of as-prepared graphene films. This can be evidenced by Dirac points showing up around V_g=~60 V in an ambient condition, implying the doping density (n) is ~ 4.26 x 10^{12} cm^{-2} before HNO_3 doping (E_D=~0.265 eV). The Fermi energy level shift measured by UPS is ~0.130 V after HNO_3 doping (Fig 3d, inset), and then the overall deduced doping level considering both etching and HNO_3 doping is calculated to be ~9.43 x 10^{12} cm^{-2} (E_D=~0.395 eV).

J. Sheet resistance enhancement by various wet chemical p-dopants

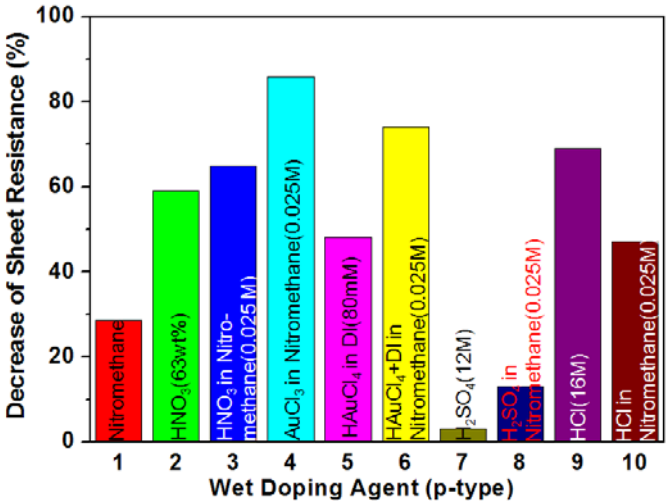

Fig S10. Decrease of sheet resistance vs. various wet doping agent. The large-area graphene can be unintentionally p-doped by etchants such as ammonium persulfate or iron chloride, leading to the low sheet resistance before additional doping. In the case of the roll-to-roll method, the sheet resistance after HNO_3 doping is decreased from 272 to 108 Ohm/sq (~59% decrease). We tested various doping agent that have been used for carbon nanotubes (*Ref*. 25 in the main text), and found that HNO_3 is suitable for practical applications.

K. High voltage *I-V* characteristics of graphene films

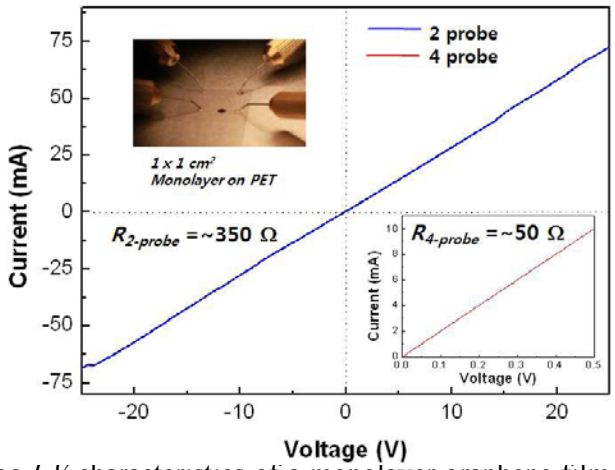

Fig S11. High voltage *I-V* characteristics of a monolayer graphene film transferred on a PET by a roll-to-roll method. The non-linear *I-V* characteristics of the graphene film on a PET substrate is not observed between V_{SD}=-25~+25 V. If V_{SD} > 30 V, The devices tend to breakdown before reaching the saturation of current probably due to deformation of PET (Tg=~150˚C) substrates by heat dissipated from the contact. In the case of SiO_2/Si substrates, the graphene film withstands V_{SD}=-50~+50 V. Considering the practical operation voltages of commercial electronic devices, V_{SD} < 20 V, the graphene electrode is expected to be reliable for most of high-voltage applications including LCD and OLED.

L. Structures of graphene-based touch screen devices

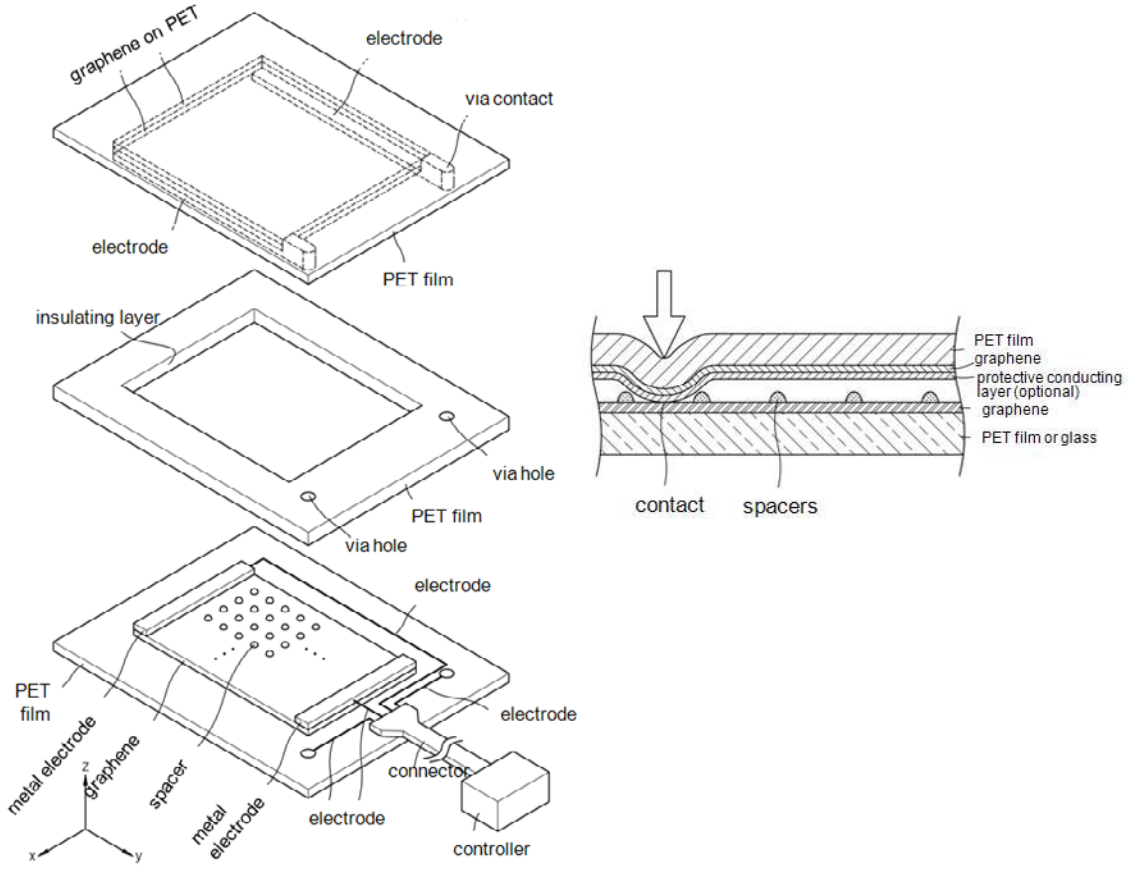

Fig. S12. Structure and working principle of graphene-based touch screen devices. The protective conducting layer was not used in the actual experiment.